红外与激光工程
INFRARED AND LASER ENGINEERING
EI, SCOPUS, CSCD等收录期刊

内部微缺陷的超声与数字全息成像检测系统设计

王星 高磊 王岩 汪海涛

Design of a hybid ultrasound and digital holography imaging system for detection of internal micro-defects

Wang Xing, Gao Lei, Wang Yan, Wang Haitao

在线阅读 View online: https://doi.org/10.3788/IRLA20190518

您可能感兴趣的其他文章

Articles you may be interested in

基于数字全息干涉技术的动态超声场成像与检测

Dynamic ultrasonic wavefield imaging and detection based on digital holographic interferometry

红外与激光工程. 2019, 48(11): 1125001–1125001(11) https://doi.org/10.3788/IRLA201948.1125001

航空复合材料内部缺陷差动式激光红外热成像检测

Detection of internal defects in aviation composites with differential laser infrared thermal imaging

红外与激光工程. 2019, 48(5): 504003–0504003(7) https://doi.org/10.3788/IRLA201948.0504003

脉冲激光周向探测地面目标捕获建模与仿真

Modeling and simulation of acquisition for ground target by pulsed laser circular-viewing detection

红外与激光工程. 2018, 47(2): 206001–0206001(11) https://doi.org/10.3788/IRLA201847.0206001

超短脉冲激光烧蚀冲量耦合测量方法

Methods of extreme short pulse laser ablation impulse coupling measurement

红外与激光工程. 2017, 46(3): 329002–0329002(7) https://doi.org/10.3788/IRLA201746.0329002

激光探测小型化收发系统设计

Design of miniaturized transmitting-receiving system for laser detection

红外与激光工程. 2017, 46(9): 906008–0906008(7) https://doi.org/10.3788/IRLA201746.0906008

激光引信窄脉冲光源驱动电路设计

Design of narrow pulse light source driving circuit of laser fuze

红外与激光工程. 2018, 47(S1): 16–22 https://doi.org/10.3788/IRLA201847.S106004

Design of a hybid ultrasound and digital holography imaging system for detection of internal micro-defects

Wang Xing[1], Gao Lei[2], Wang Yan[3], Wang Haitao[1]

(1. China Coal Energy Reserach Institute Co. Ltd., Xi'an 710054, China;
2. General Standard (Beijing) Institute of Science and Technology, Beijing 100070, China;
3. Xi'an University of Science and Technology, Xi'an 710054, China)

Abstract: Non-contact detection of internal micro-defects of the micro-electro-mechanical system and minimechanism required a high accuracy and strong penetration test. The current detection methods were difficult to achieve high precision while also having strong penetrating power. In response to the above problems, a composite system of ultrasonic detection and digital holography imaging was designed. Ultrasonic detection technology had strong penetrating power, and digital holographic imaging had higher resolution. The composite system designed included a near-field ultrasonic subsystem, an digital holographic subsystem and a synchronous control subsystem. In the near-field ultrasonic subsystem, the generated near-field ultrasonic wavefields passed through the internal defect of the sample and formed the surface ultrasonic wavefield on the surface of the sample. The digital holographic subsystem mainly measured and analyzed the transient morphology of the surface ultrasonic wavefields, and the internal defect information contained in the surface ultrasonic wavefield could be analyzed. The experimental results show that the system can measure the transient 3D topography of the ultrasonic wavefield by analyzing the ultrasonic wavefield, and can effectively detect internal defects of 50 μm.

Key words: digital holographic interferometry; pulsed laser; near-field ultrasonic wavefield; internal defects

CLC number: TH741 **Document code:** A **DOI:** 10.3788/IRLA20190518

内部微缺陷的超声与数字全息成像检测系统设计

王 星[1], 高 磊[2], 王 岩[3], 汪海涛[1]

(1. 中煤能源研究院有限责任公司, 陕西 西安 710051;
2. 环宇通标 (北京) 科学技术研究院, 北京 100070;
3. 西安科技大学, 陕西 西安 710054)

摘 要: 微机电系统与微机械零件的内部微缺陷需要高精度、强穿透性的非接触检测技术。目前缺少这样内部微缺陷的检测方法。针对上述问题,设计了超声与数字全息成像的复合系统。该系统结合了超声检测的强穿透能力和数字全息成像技术的高分辨率。该系统包括近场超声子系统、数字全息子系统和同步控制子系统。在近场超声子系统中,产生的近场超声波场穿过样品的内部缺陷,在样品表面形成表面超声波场,再通过数字全息子系统测量和分析这个表面超声波场的瞬态形貌,分析声波场中包含的内部缺陷信息。实验结果表明:该系统通过对超声波场的分析,可以测量出超声波场的瞬态三维形貌,并且可以有效的检测出 50 μm 的内部缺陷。

关键词: 数字全息干涉术; 脉冲激光; 近场超声波场; 内部缺陷

收稿日期:2019−11−10; **修订日期:**2020−01−05

基金项目:陕西省教育厅专项科研计划项目 (19JK0537);陕西省自然科学基础研究计划项目 (2019JQ-791)

作者简介:王星 (1989−), 女, 工程师, 博士, 主要从事智能化检测技术方面的研究。Email:yigekongge@qq.com

0 Introduction

Non-contact detection of internal defects of the micro-electro-mechanical system (MEMS) and minimechanism requires a high accuracy and strong penetration test[1]. Most of these defects are micro-nano and very difficult to detect.

There are already some techniques for detecting subsurface defects in MEMS and minimechanism. X-ray, ultrasonic microscopy and scanning near-field acoustic holography can all evaluate small internal defects, but they have different imaging methods and evaluations.

Germany's Fein Focus X-ray imaging technology can achieve a horizontal resolution of one micron, but no three-dimensional imaging capabilities[2]. In recent years, the latest 3D X-Ray CT has been developed to achieve extremely high resolution (50 nm)[3]. However, the test sample must be cut into small samples to image, and the imaging efficiency is extremely low. The X-ray method is difficult to detect for closed cracks and delamination defects perpendicular to the ray direction inside the sample.

Shekhawat and David of Northwestern University developed a scanning near-field ultrasound holography (SNFUH) technique based on atomic force microscopy[4]. SNFUH technology not only can further improve spatial resolution, but also achieve subsurface defect imaging[5]. But SNFUH technology can only scan very small sample areas, imaging speed is very slow, and can not three-dimensional imaging of defects. Therefore, this technique is also not suitable for the detection of internal defects in micromechanical structures.

Scanning acoustic microscopy (SAM) enables tomographic imaging of internal defects in samples by point-by-point scanning of high-frequency ultrasound focusing probes[6]. However, SAM can only detect very thin samples. The super-resolution 3D acoustic microscopy imaging technology developed by Professor Zhang Guangming of Liverpool John Morris University has overcome the problem of wavelength limitation of the longitudinal resolution of SAM[7]. Although the technology for scanning acoustic microscopy is currently used for chip inspection, its resolution is far from meeting the detection requirements of modern microelectronic packages and micromechanical structures.

In summary, the SAM technology utilizes the characteristics of high-frequency ultrasonic waves, and has high longitudinal resolution and strong penetrating power. However, the ultrasound probe that receives the ultrasound wavefields affects the lateral resolution of the detection. The high frequency ultrasonic focusing probe is generally composed of a plurality of independent piezoelectric array elements, and the focus position and the direction of the ultrasonic beam are adjusted according to a certain rule and time delay[8]. The lateral resolution of the ultrasonic focusing probe is affected by the size and arrangement of the piezoelectric elements. For example, the most advanced scanning acoustic microscope, even with the highest frequency (300 MHz) ultrasonic focusing probe, can only achieve a lateral resolution of more than ten micrometers.

Optical methods are used to replace ultrasonic probes to receive ultrasound, many of the challenges (such as component density, component spacing, and aperture) of current ultrasonic transducer arrays can be overcome, and imaging performance can be improved. Compared to the mechanical sorting of array elements in an ultrasound transducer array, the ordering of pixel elements in optically charge coupled devices (CCDs) is much more precise, and the use of optical imaging techniques to receive ultrasound is the future and trend of MEMS and minimechanism detection[9].

The optical method used to detect the ultrasonic signal can be divided into two types: one is the non-interference method, such as the slit method[10]. Besides, the photodetector is used to pick up the optical signal, which takes the single point or multi-point collection, but this collection is not the full-field collection. In this case, this method cannot fully measure the dynamic ultrasonic wavefield. The other one is the interference method,

including electron speckle interference[11]. Conventional electronic speckle pattern interferometry is used to measure vibrations. In recent years, speckle interferometry techniques have also been proposed in non-contact detection of ultrasound signals, including real-time electronic speckle pattern interferometry and pulsed electronic speckle pattern interferometry[12]. Pulse-electronic speckle interferometry is based on a pulsed laser system, and dual pulse or multi-pulse lasers have a great advantage in applying non-contact measurements to ultrasound[13−14]. At the same time, this technology requires the optical path system with significantly high accuracy[15]. There are methods of using Fabry-Perot interferometer and photorefractive interferometer, but the former is unstable, while the latter is very expensive[16].

Based on the above ideas, a composite system of near-field ultrasonic detection and digital holography imaging is designed in this paper to detect interal defects. Pulsed holography has shown its superiorities in recording fast events with high time resolution[17]. An angular multiplexing technique may be adopted to record a series of holograms in a time sequence to study the dynamics of a fast event[18]. However, this optical path of pulsed holography is complex and difficult to be adjusted in the experiment. Aiming at internal defects of the MEMS and minimechanism, this paper designs a composite system for mearsing near-field ultrasonic wavefield by digital holographic interferometry. The system consists a near-field ultrasonic subsystem, an digital holographic subsystem and a synchronous control subsystem. The performance of the designed composite system is tested on the standard resolution test target and minimechanism.

1 Working principle of composite system

The composition of the composite system is shown in Fig.1. The system mainly includes three subsystems, a digital holographic subsystem, an near-field ultrasounic subsystem and a synchronous control subsystem. The digital holographic subsystem further includes an light path of digital holographic microscopy, charge coupled device (CCD)and pulsed laser. The main task of the digital holographic subsystem is to use the digital holography technology to capture the hologram of the ultrasonic wavefield. The near-field ultrasounic subsystem includes an arbitrary waveform generator, power amplifier, ultrasonic transducer, and oscilloscope. The primary purpose of the near-field ultrasounic subsystem is to generate an ultrasound field for detecting defects. The synchronous control subsystem mainly makes the digital holographic subsystem and the near-field ultrasounic subsystem cooperate with each other.

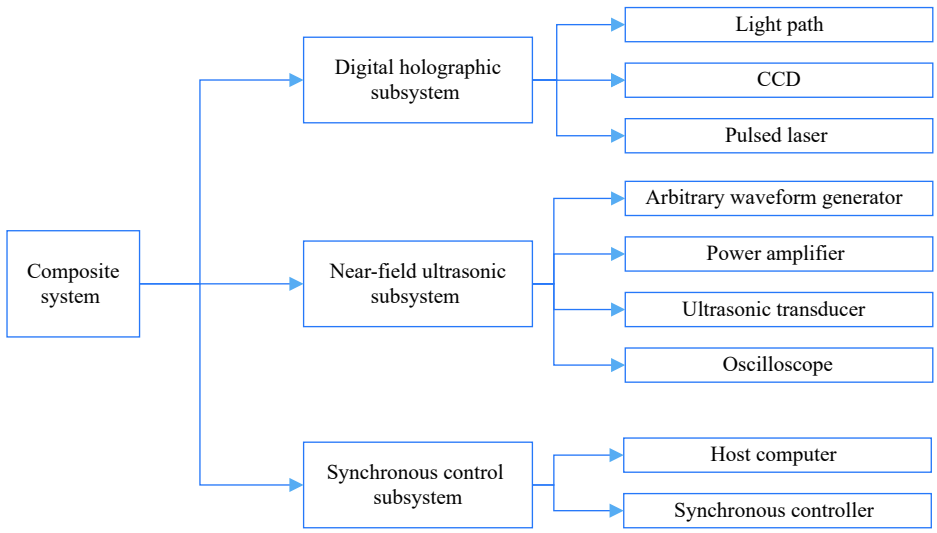

Fig.1 Overall design of the system

The schematic diagram of the detection principle of the system is shown in the Fig.2. First, the ultrasonic transducer is placed at the bottom of the test sample, and an excitation signal is provided by the synchronous control system to generate an ultrasonic signal by the ultrasonic transducer. The ultrasonic waves form the dynamic ultrasonic wavefields that propagate through the coupling medium to the bottom of the solid sample, then propagates from the bottom to the inside of the sample. The ultrasonic wavefields pass through the internal defect of the sample, causing corresponding changes. The ultrasonic wavefields contains information of internal defect and propagate to the surface of the sample, and form the corresponding deformation on the surface of the sample. Second, the synchronous control system separately energizes the pulsed laser and the CCD by setting an appropriate delay time. The pulsed laser is irradiated onto the surface of the sample through the light path, and the information of the ultrasonic wavefields are transmitted to the digital holograms.

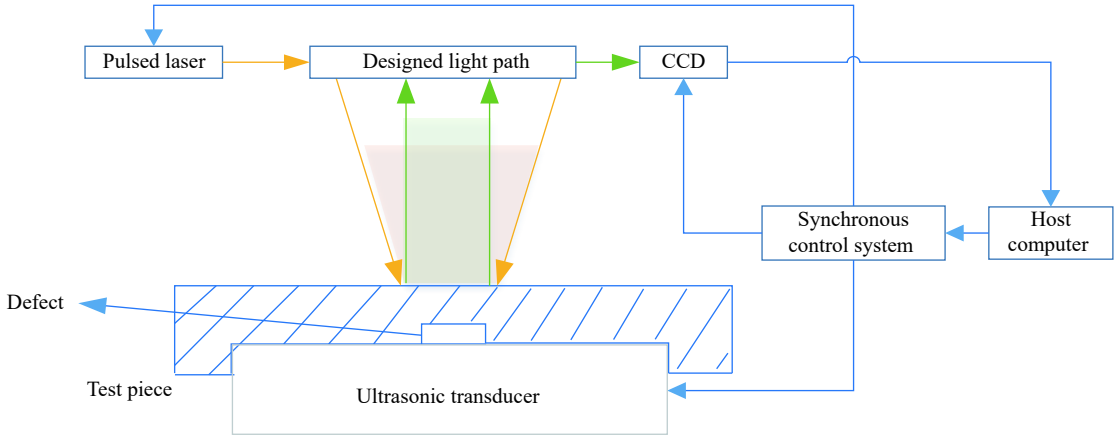

Fig.2 Schematic diagram of defect detection

2 Digital holography subsystem

In order to capture high-frequency transient ultrasonic wavefields, a pulsed laser is used to replace a continuous laser as the system light source. In this paper, the NIMMA 400 Pulsed Laser ($\lambda = 532$ nm) from Beamtech with a pulse width of 8 ns is used since our targeted application is for measurement of transient ultrasonic wavefields in ultrasonic non-destructive testing. Important parameters for the high-speed camera include the shutter speed, CCD sensor sensitivity and signal to noise ratio (SNR) and the frame rate. The exposure time of the CCD camera should be as short as possible in order to match the pulse width of the pulsed laser. The larger exposure time introduces unwanted light from the experimental environment into the hologram, which degrade the quality of the hologram. In this paper, the CCD (German PCO Company 1 600 model) with an exposure time of 500 ns.

The digital holography subsystem as shown in Fig.3 is designed, where four beam splitters are used to adjust the directions of the object light and the reference light, and the stray light (Red arrow)can be excluded from the light path. First of all, the pulsed light beam passes through half-waveplate and Glan prism. They can not only control the energy of the light beam, but also ensure the pure polarized light beam. In order to facilitate the ratio of reference beam to object beam intensity, a ratio of 9∶1 non-polarizing beam splitter cube (NPBS) is chosen as the beam splitter -1. The NPBS used here is 90% of the transmitted light and 10% of the reflected light, which enhances the intensity of the object light and weakens the intensity of the reference light.

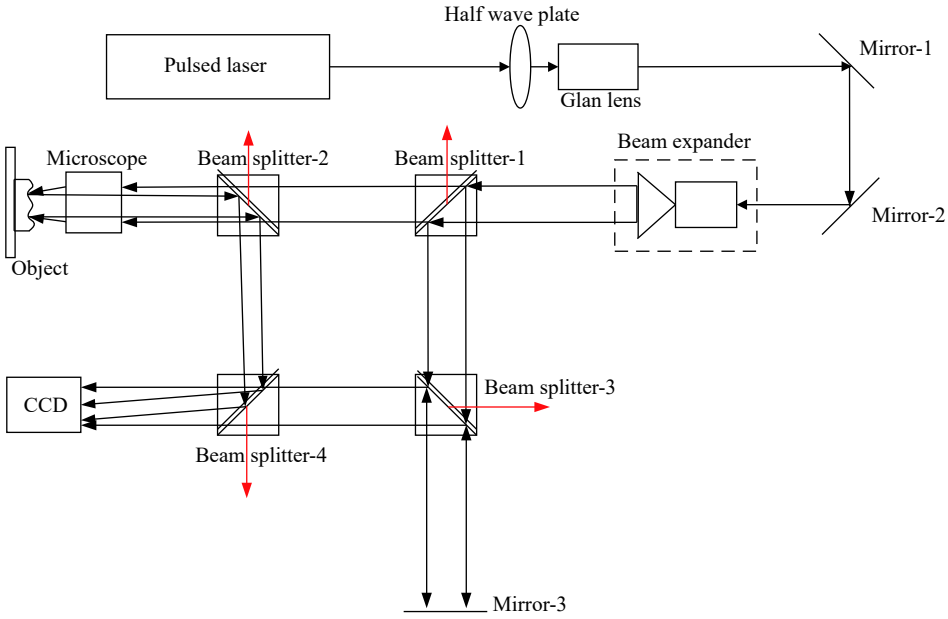

Fig.3 Design of the digital holography subsystem

3 Near-field ultrasonic subsystem

The purpose of the ultrasound subsystem is to generate a single-frequency narrow-pulse near-field longitudinal wave. The subsystem consists of an arbitrary waveform generator, power amplifier, ultrasonic transducer, and oscilloscope. The system produces a single-frequency narrow-pulse near-field ultrasound in the test sample and produces a uniform near-field ultrasonic longitudinal wave. The main component of the near-field ultrasonic longitudinal wave is the evanescent wave, which can overcome the diffraction limit of the traditional far-field ultrasonic imaging, so that the lateral resolution of the near-field ultrasonic imaging is no longer limited by the ultrasonic wavelength, and can achieve higher resolution.

The 4-6 period sinusoidal pulse signal is used by the system to excite the near-field ultrasonic probe to produce single-frequency narrow pulse near-field longitudinal wave, and the defect size can be detected is tens of microns.

4 Synchronous control subsystem

Control and synchronization is fundamental for high-quality hologram capture. The control system needs to provide a precise delay time between the laser pulse and the camera capture and ultrasonic signal for the proposed digital holography subsystem. The synchronous control system is shown in Fig.4, consisting of a host computer, a synchronous controller, the CCD camera, ultrasonic signal and the pulsed laser. The synchronous controller is implemented through the timing of NI's PXI-6602 and digital I/O modules.

As shown in Fig.5, the synchronous controller is designed to ensure the CCD camera receives the 8 ns laser pulse with its 500 ns exposure time window. The laser and CCD camera is set up into the external control state. The clock signal of the synchronous controller will coincide with the external control signal, and the external signal control line will be connected to the laser and the CCD camera. At the same time, in order to set the delay time at the optimum value, the control system's initialization and control port's definition have to be done.

By changing the delay time and repeating the measurement process, the ultrasonic wavefields at different times on the surface of the sample can be obtained. By designing suitable time series, the array data of ultrasonic wavefields surface topography can be obtained. Each data array forms the ultrasonic wavefields

sample. The size of the two space is determined by the number of components of the CCD sensor. At each spatial position in the array, the acquired data is the ultrasonic signal at this time, which is equivalent to the A-scan signal in the conventional ultrasonic nondestructive testing.

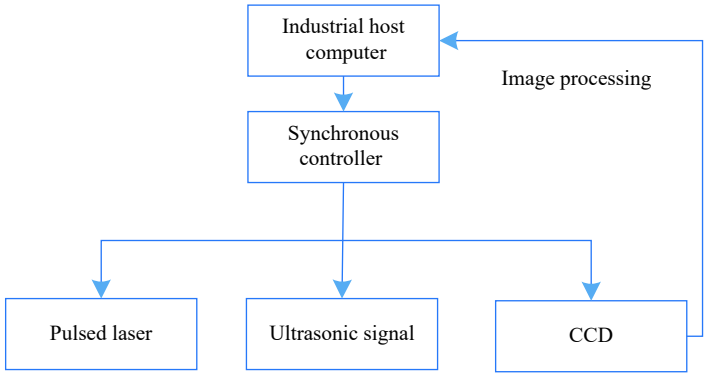

Fig.4 Schematic of the synchronous control system

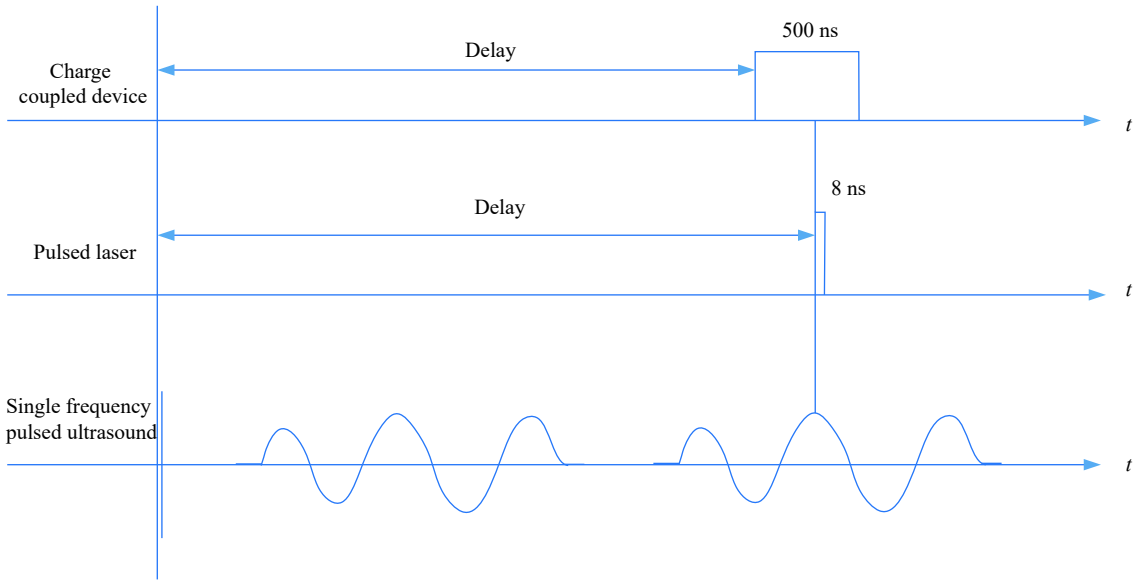

Fig.5 Schematic diagram of system timing

The sampling frequency of the ultrasonic signal is determined by the step of the delay time. The minimum step of the delay time is the pulse length of the laser pulse. If the step of the delay time is less than the pulse width of the laser pulse, the ultrasonic wavefields will overlap and fail. Therefore, the laser pulse width determines the upper limit of the sampling frequency for the system to acquire the ultrasonic signal.

5 Experimental verification

In this paper, designed digital holography subsystem is shown in Fig.6. The sample designed in this experiment is shown in Fig.7, and the sample material is aluminum alloy. The groove of the ultrasonic excitation surface is circular, so that the ultrasonic transducer can be embedded in the sample to facilitate ultrasonic excitation of the bottom of the sample. A flat-bottomed hole having a diameter of 50 μm and a depth of 0.1 mm was machined at the center of the sample according to the detection requirements. This hole trap represents an internal defect in the micromechanical structure. The thickness of the sample to be tested is 0.3 mm.

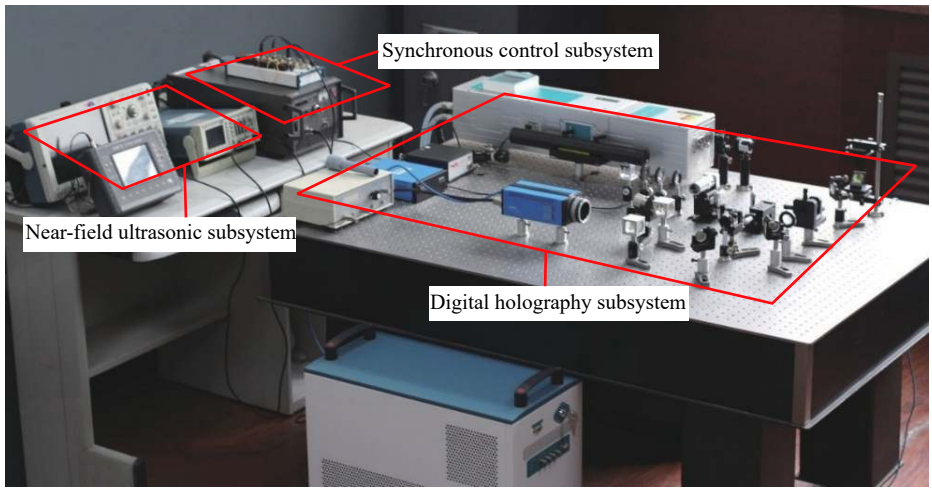

Fig.6 Designed digital holography subsystem

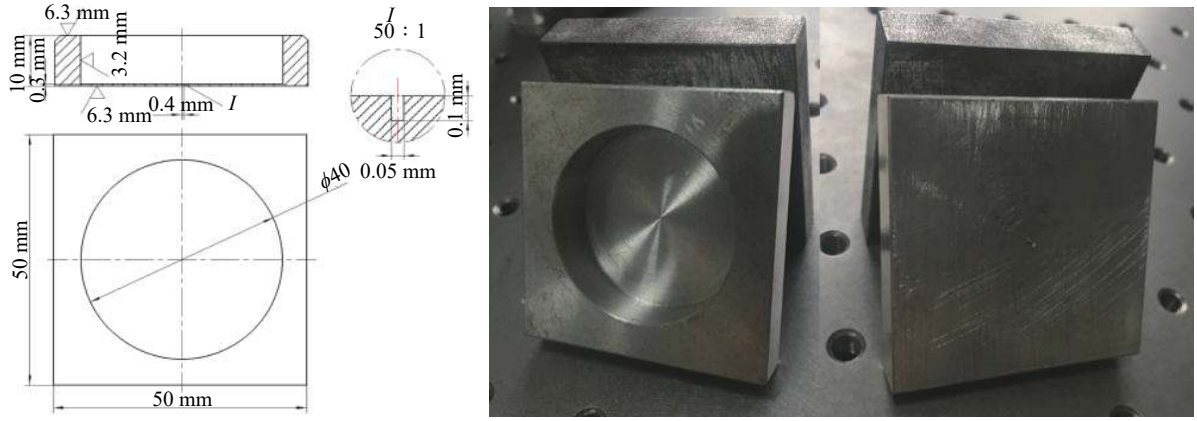

Fig.7 Test sample

The sample shown in Fig.7 was tested. The detection system used is shown in Fig.6. The microscope used in this experiment is Mitutoyo, Japan. The magnification is 50X, the working distance of the microscope is 13 mm, the recording distance is 500 mm, and the ultrasonic excitation signal is 5 MHz.

As shown in Fig.8, the ultrasonic wavefields morphology of the sample at different times are recorded separately in this experiment. Two different delay times ($t1$, $t2$) are set respectively, the maximum amplitude moment of the ultrasonic wavefields is recorded at time $t1$, and the maximum amplitude moment of the negative direction of the ultrasonic wavefields is recorded at time $t2$. In order to compare the defective and non-defective conditions, under the same conditions, the surface ultrasonic wavefields of the sample without defects was recorded at the corresponding time ($t1$, $t2$).

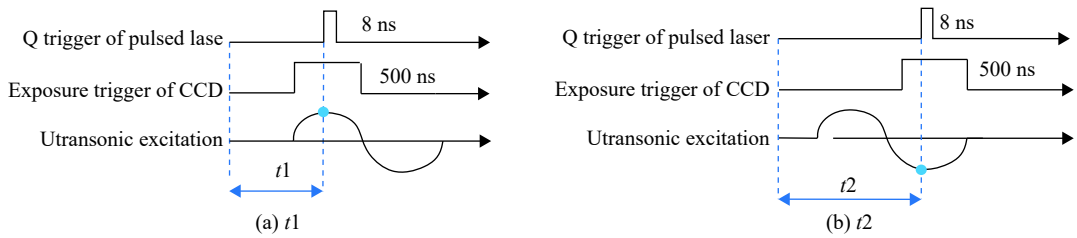

Fig.8 Synchronous control timing diagram: (a)$t1$; (b)$t2$

This paper first measured aluminum sheets with no defects (0.3 mm thick). The measurement principle is shown in Fig.2, and the detection system is shown in Fig.6. In this experiment, the ultrasonic wavefields are measured at time points $t1$ and $t2$, as shown in Fig. 9.

As shown in Fig.9, the ultrasonic wavefields on the surface of the aluminum plate does not change significantly at times $t1$ and $t2$, and is close to the flat surface. Because this experiment added a high power microscope, the recorded spot size is very small, so the shape variable of the entire ultrasonic wavefields is close to the flat surface in the spot size. The ultrasonic wavefields morphology measured in Fig.9 is small enough that its phase is not wrapped by [-π, π], and the interferogram does not need to be unwrapped.

Secondly, this experiment tests the defects described in Fig.7. Figure 10 shows the surface topography of the ultrasonic wavefields at time $t1$.

As can be seen from the Fig.10, compared with the defect-free ultrasonic wavefields topography in Fig. 9(a), there is a relatively obvious deformation in the results of this measurement. The deformation of the middle protrusion corresponds to the center position of the internal defect, and the protrusion gradually becomes smaller as the delay time changes.

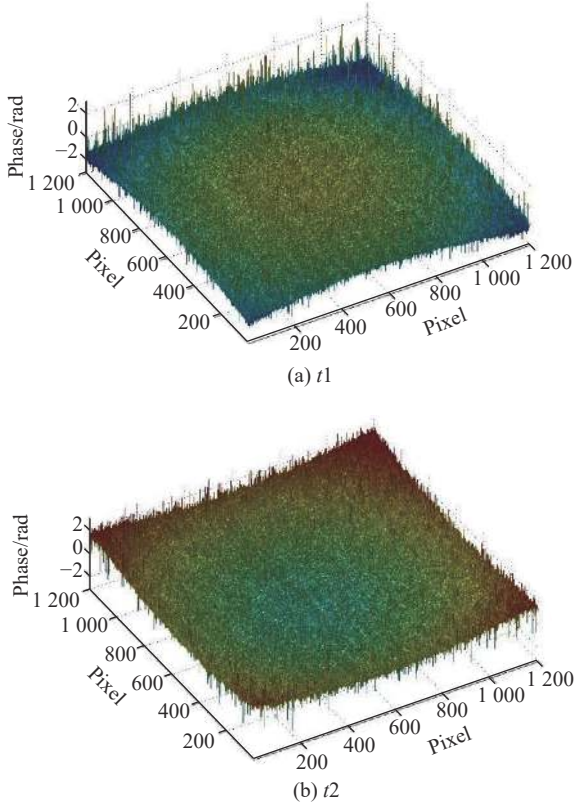

Fig.9 Ultrasonic wavefields morphology of aluminum sheet without defect: (a)$t1$; (b)$t2$

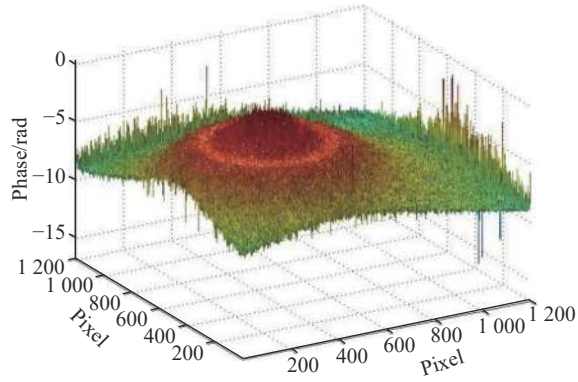

Fig.10 Ultrasonic wavefields surface topography at $t1$

In order to analyze the accuracy of the method and experimental system, this paper extracts the one-dimensional cross-section data on the two-dimensional ultrasonic wavefields data. The cross section is shown in Fig.11, where x = 600 and y = 600.

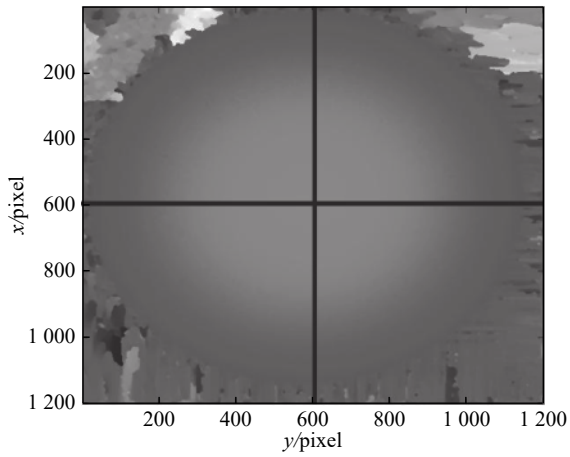

Fig.11 Extraction of one-dimensional data

The amplitude of the ultrasonic wavefields can be calculated. This paper compares the one-dimensional cross-section data at time $t1$ without defects and defects, and the results are shown in Fig.12.

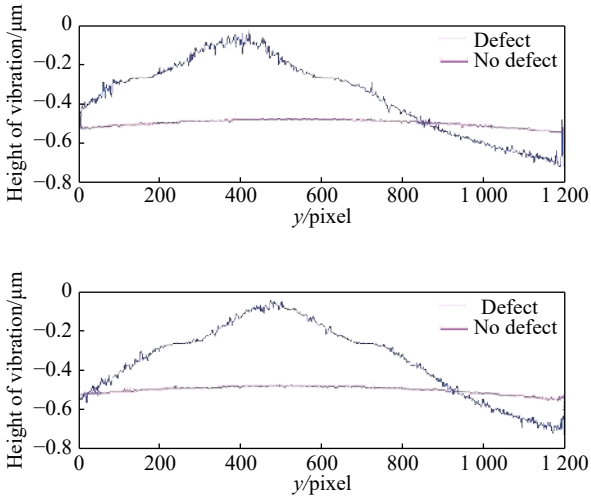

Fig.12 Data comparison at time $t1$

As shown in Fig.12, the blue is the morphology of the ultrasonic wavefields in the defective area, and the red is the morphology of the ultrasonic wavefields without defects. Figure 12 shows the cross-section data measured at the $t1$ delay time, and the maximum value of the amplitude change is 0.55 μm. It can be seen that when there is no defect, the shape of the ultrasonic wavefields changes very small, and close to a straight line. In the case of defects, the middle area will bulge and the surrounding area will be concave. The amount of change in amplitude measured in this experiment is the difference between the highest point and the lowest point in the measurement range, which is different from the actual amplitude.

The same as the method of measuring the ultrasonic wavefields at time $t1$, the data of the transient ultrasonic wavefields at time $t2$ can be obtained. The surface morphology of the ultrasonic wavefields at time $t2$ shows in Fig.13.

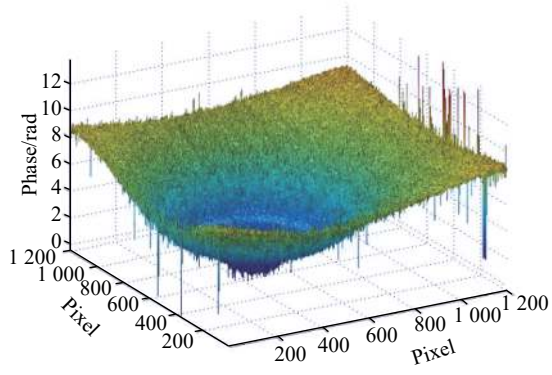

Fig.13 Ultrasonic wavefields surface topography at $t1$

Similarly, the measurement data at time $t2$ is quantitatively analyzed. The result is shown in the Fig.14.

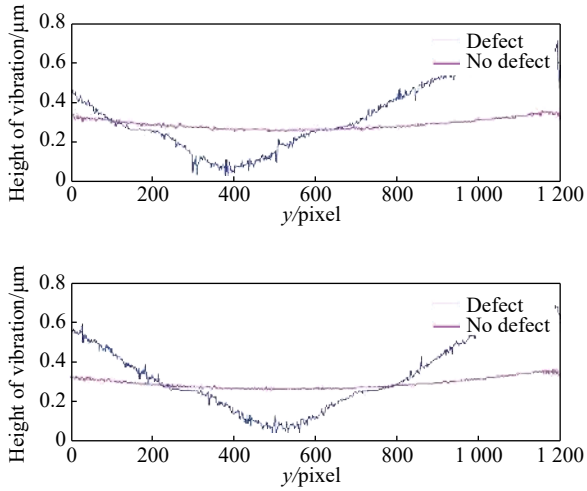

Fig.14 Data comparison at time $t2$

In the Fig.14, blue is the morphology of the ultrasonic wavefields of the defective area, and red is the morphology without defects. Figure 14 shows the cross-section data measured at time $t2$, and the magnitude of the change is up to 0.46 μm. It can be seen that when there is no defect, the shape of the ultrasonic wavefields changes in a small range close to a straight line. Deformation can occur in a defective place.

Table 1 is the maximum amplitude of the two transient

Tab.1 Maximum amplitude of dynamic ultrasonic wavefields

Time point of measurement	$t1$	$t2$
Maximum amplitude of transient ultrasonic wavefield with defects/μm	0.55	0.46
Maximum amplitude of transient ultrasonic wavefield without defects/μm	0.11	0.11
Deformation of ultrasonic wavefield due to defects/μm	0.44	0.35

ultrasonic wavefields obtained in this experiment. If the maximum amplitude of the transient ultrasonic wavefields with defects is used to reduce the maximum amplitude of the transient ultrasonic wavefields without defects, as shown in Tab. 1, the maximum value due to internal defects can be obtained.

6 Conclusions

In order to measure dynamic ultrasonic wavefields and detect internal defects, The composite system of ultrasonic detection and digital holography imaging is designed in this paper. The main features and advantages of the designed system include: (1) An novel digital holographic subsystem prevents the unwanted light into the CCD camera and also strengths the object light which is weak due to reflection; (2) The system uses a pulsed laser, which has a shorter coherence distance so that the system reduces the interference from the rest of the coherent light; (3) Due to the use of a short exposure time (500 ns) CCD camera and a pulsed nano-second laser, the designed system can be used for static and dynamic 3D characterization, and measurement of ultrasonic wavefields; (4) Near-field ultrasound subsystem overcomes the diffraction limit of traditional ultrasound and improves the resolution of internal defect detection; (5) The composite system can image the high-frequency ultrasonic wavefields in the full field, instead of the traditional point-by-point scanning, and realize the recognition of internal defects by analyzing the sound field image.

The performance of the designed system is tested using the standard resolution test target and test sample containing micron internal defect. The results of the experiment show that the transient three-dimensional topography of the dynamic ultrasonic wavefields is measured at different moments and internal defects can be effectively detected. In the future, more applications will be carried out to analyze the size and location of internal defects.

References:

[1] Zhou Z, Zhang K, Zhou J, et al. Application of laser ultrasonic technique for non-contact detection of structural surface-breaking cracks [J]. ***Optics & Laser Technology***, 2015, 73: 173−178.

[2] Boone M A, Nielsen P, De K T, et al. Monitoring of stainless-steel slag carbonation using X-ray computed microtomography [J]. ***Environmental Science & Technology***, 2014, 48(1): 674−680.

[3] Hapca S, Baveye P C, Wilson C, et al. Three-dimensional mapping of soil chemical characteristics at micrometric scale by combining 2D SEM-EDX data and 3D X-Ray CT images [J]. ***Plos One***, 2015, 10(9): e0137205.

[4] Shekhawat G S, Avasthy S , David V P. Probing buried defects in extreme ultraviolet multilayer blanks using ultrasound holography [J]. ***Nanotechnology***, 2010, 6(9): 671−674.

[5] Dravid V. Seeing the invisible: Scanning near-field ultrasound holography (SNFUH) for high resolution sub-surface imaging [J]. ***Microscopy & Microanalysis***, 2013, 13(2): 1220−1221.

[6] Doherty M, Sykes J M. Micro-cells beneath organic lacquers: a study using scanning Kelvin probe and scanning acoustic microscopy [J]. ***Corrosion Science***, 2004, 46(5): 1265−1289.

[7] Zhang G M, Harvey D M, Burton D R. Micro-nondestructive evaluation of microelectronics using three-dimensional acoustic imaging [J]. ***Applied Physics Letters***, 2011, 98(9): 102110.

[8] Kumazawa T, Toshiba K K. Ultrasound probe diagnosing apparatus, ultrasound diagnostic apparatus, and ultrasound probe diagnosing method:Japan,1839579A[P], 2007-10-03.

[9] Wang X, Zhang G M, Ma H, et al. Measurement of a 3D ultrasonic wavefield using pulsed laser holographic microscopy for ultrasonic nondestructive evaluation [J]. ***Sensors***, 2018, 18(2): 573.

[10] Pelivanov I, Shtokolov A, Wei C, et al. A 1 kHz a-scan rate pump-probe laser-ultrasound system for robust inspection of composites [J]. ***IEEE Transactions on Ultrasonics, Ferroelectrics, and Frequency Control***, 2015, 62(9): 1696−1703.

[11] Abolhassani M, Rostami Y. Speckle noise reduction by division and digital processing of a hologram [J]. ***Optik - International Journal for Light and Electron Optics***, 2012, 123(10): 937−939.

[12] Vladimirov A P, Kamantsev I S, Veselova V E, et al. Use of dynamic speckle interferometry for contactless diagnostics of fatigue crack initiation and determining its growth rate [J].

Technical Physics, 2016, 61(4): 563−568.

[13] Cai X O, Lai X J. Study on information content of the 3D object's coherent imaging and hologram information redundancy [J]. ***Optik - International Journal for Light and Electron Optics***, 2012, 123(3): 240−245.

[14] Melninkaitis A, Tamosauskas G, Balciunas T, et al. Time-resolved off-axis digital holography for characterization of ultrafast phenomena in water [J]. ***Optics Letters***, 2008, 33(1): 58.

[15] Hong K M, Kang Y J, Choi I Y, et al. Ultrasonic signal analysis according to laser ultrasound generation position for the detection of delamination in composites [J]. ***Journal of Mechanical Science and Technology***, 2015, 29(12): 5217−5222.

[16] Yang C, Yan X, Zhu R, et al. Diffraction study of volume holographic gratings in dispersive photorefractive material for femtosecond pulse readout [J]. ***Optik - International Journal for Light and Electron Optics***, 2010, 121(12): 1138−1143.

[17] Lee Y L, Lin Y C, Tu H Y, et al. Phase measurement accuracy in digital holographic microscopy using a wavelength-stabilized laser diode [J]. ***Journal of Optics***, 2013, 15(15): 5403.

[18] Cao L, Wang Z, Zhang H, et al. Volume holographic printing using unconventional angular multiplexing for three-dimensional display [J]. ***Applied Optics***, 2016, 55(22): 6046.